THE JOURNAL OF PHYSICAL CHEMISTRY A
A JOURNAL OF THE AMERICAN CHEMICAL SOCIETY

pubs.acs.org/JPCA

Article

Interaction of Th with $H^{0/-/+}$: Combined Experimental and Theoretical Thermodynamic Properties

Monica Vasiliu, Kirk A. Peterson, Mary Marshall, Zhaoguo Zhu, Burak A. Tufekci, Kit H. Bowen,* and David A. Dixon*

Cite This: *J. Phys. Chem. A* 2022, 126, 198−210

Read Online

ACCESS | Metrics & More | Article Recommendations | Supporting Information

ABSTRACT: High-level electronic structure calculations of the low-lying energy electronic states for ThH, ThH^-, and ThH^+ are reported and compared to experimental measurements. The inclusion of spin−orbit coupling is critical to predict the ground-state ordering as inclusion of spin−orbit switches the coupled-cluster CCSD(T) ordering of the two lowest energy states for ThH and ThH^+. At the multireference spin−orbit SO-CASPT2 level, the ground states of ThH, ThH^-, and ThH^+ are predicted to be the $^2\Delta_{3/2}$, $^3\Phi_2$, and $^3\Delta_1$ states, respectively. The adiabatic electron affinity is calculated to be 0.820 eV, and the vertical detachment energy is calculated to be 0.832 eV in comparison to an experimental value of 0.87 ± 0.02 eV. The observed ThH^- photoelectron spectrum has many transitions, which approximately correlate with excitations of Th^+ and/or Th. The adiabatic ionization energy of ThH including spin−orbit corrections is calculated to be 6.181 eV. The natural bond orbital results are consistent with a significant contribution of the Th^+H^- ionic configuration to the bonding in ThH. The bond dissociation energies for ThH, ThH^-, and ThH^+ using the Feller−Peterson−Dixon approach were calculated to be similar for all three molecules and lie between 259 and 280 kJ/mol.

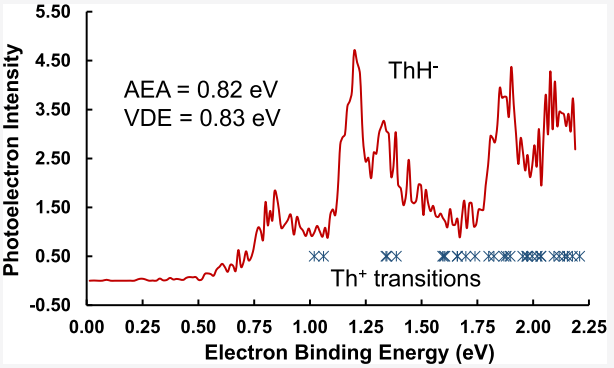

INTRODUCTION

There is significant interest in the properties of the actinides and actinide-containing species due to their unique and interesting chemical behavior and their importance in nuclear fuel development. Especially, for Th, seen as the bridge between transition metals and the actinide block, it is important to determine whether Th has a more transition metal-like behavior or an actinide-like behavior. Tang et al.[1] combined photoelectron spectroscopy (PES) and the MC-DHF (multiconfigurational Dirac−Hartree−Fock) computational method with a large basis set to show that the first peak in the photoelectron spectrum of Th^- is due to a transition from the first excited spin−orbit state of the anion to the ground state of the neutral atom; this electron binding energy (EBE) is 0.382 ± 0.025 eV. The experimental adiabatic electron affinity (EA) for Th is 0.607690(60) eV. Dixon, Bowen, and co-workers predicted a value of 0.59 eV for the adiabatic EA(Th) at the CCSD(T)/CBS limit using aug-cc-pwCVnZ correlation-consistent basis sets with an effective core potential for Th in a study of Th_xO_yAu clusters.[2] Peterson, Bowen, and co-workers went beyond the CCSD(T) level of theory together with all-electron four-component relativistic treatments of spin−orbit coupling to obtain a value of 0.565 eV for the EA of Th.[3]

Armentrout and co-workers[4] have experimentally determined the bond dissociation energy (BDE) of ThH^+ to be 2.45 ± 0.07 eV (forming Th^+ + H) from the reaction of Th^+ with H_2. At the CCSD(T) level with a large correlation-consistent basis set but not including spin−orbit effects, they predicted the $^1\Sigma^+$ ($\sigma^2\sigma^2$) configuration to be the ground state for ThH^+ with the $^3\Delta_1$ ($\sigma^2\sigma\delta$) state being 0.05 eV higher in energy. Using an approximate empirical-based spin−orbit correction, they obtained a BDE of 2.72 eV at the CCSD(T)/CBS-cc-pwCVnZ-DK3 level for the $^3\Delta_1$ state; they assigned this state as the ground state of ThH^+. The experimental BDE that they obtained was consistent with a previous study of Armentrout and co-workers on the reaction of Th^+ + CH_4 who obtained a value of the BDE as ≥2.25 ± 0.18 eV.[5] In this latter work, the authors performed BDE calculations at the CCSD(T) level with a triple-zeta level basis set and an approximate spin−orbit correction obtaining results similar to their later work. Andrews and co-workers[6] reacted Th atoms with H_2, D_2,

Received: August 27, 2021
Revised: December 21, 2021
Published: January 6, 2022

HD, and H_2/D_2 gas mixtures to produce ThH_xD_y neutrals in Ar and Ne matrices. Formation of ThH and ThD was favored at low concentrations and high laser power as extra energy is required in the endothermic reactions to produce ThH/D. The vibrational frequency for ThH was measured in Ne and Ar matrices with respective values of 1511.0 and 1485.2 cm^{-1}. Bowen and co-workers[7] determined that ThH_5 is an actinide-containing superhalogen molecule using a combination of PES and electronic structure calculations. The experimental vertical detachment energy (VDE) of ThH_5^- is 4.09 eV.

We are interested in understanding the fundamental interactions of actinides with different ligands. In the current work, we report the photoelectron spectrum of ThH^- and detailed computational results on the interaction of thorium atoms with the simplest ligand, hydrogen, in three different oxidation states as $H^{-/0/+}$. The methods that we employ have been used to predict a range of thermodynamic properties of Th-containing cations and molecules including $ThO^{+/0}$,[8] $THN^{+/0}$,[9] $ThCO^{+/0}$,[10] and $ThO_2^{+/0}$,[11] where the agreement with experiments is usually within ±4 kJ/mol and always within the experimental error limits. Similar excellent agreement has been found between experimental and calculated values for ThX_2 and ThX_4 for X = F and Cl.[12]

EXPERIMENTAL AND COMPUTATIONAL METHODS

Experimental Section. The ThH^- and ThD^- anions were produced and analyzed using a house-built anion photoelectron spectrometer, which has been described in detail previously.[13] The apparatus consists of an ion source, a time-of-flight mass spectrometer, a Nd:YAG photodetachment laser, and a magnetic bottle energy analyzer. The thorium hydride anions were generated in a laser vaporization ion source. A rotating, translating thorium rod was ablated using the second harmonic of an Nd:YAG laser (532 nm and 2.33 eV), while 20 psi of UHP H_2 gas expanded over the Th rod. After pulsing H_2 gas over the rod for a minute, the gas flow was shut off, and the experiments were conducting using no backing gas. In order to generate the ThD^- anions, the experiment was repeated with 15 psi of D_2 expanded over the Th rod. The resulting anions were then extracted before entering the photodetachment region.

Anion PES experiments were conducted by crossing a mass-selected anion beam with a fixed-frequency photon beam and energy analyzing the resulting photodetached electrons. The photodetachment process is governed by the energy conservation relationship, $h\nu$ = EBE + EKE, where $h\nu$ is the photon energy, EBE is the electron binding energy, and EKE is the electron kinetic energy. The second (532 nm = 2.33 eV) harmonic of an Nd:YAG laser was used to photodetach electrons from the Th^-, ThH^-, and Th^- anions. The photoelectron spectra were calibrated against the known transitions of Cu^-.[14] The resolution of the magnetic bottle energy analyzer is ~50 meV at 1 eV EKE.

Computational Methods. The geometries were optimized, and the harmonic frequencies (ω_e) and anharmonic constants ($\omega_e x_e$) of the diatomic neutral ThH, anion ThH^-, and cation ThH^+ were obtained at the CCSD(T)[15−18] (coupled-cluster theory with single and double excitations with a perturbative triple correction) level with the third-order Douglas−Kroll−Hess Hamiltonian (DKH3).[19−21] The aug-cc-pV*n*Z-DK for H[22,23] and the cc-pwCV*n*Z-DK3 for Th[24] for n = D, T, and Q basis sets were used; these are denoted as aw*n*-DK. These calculations included the correlation of the valence electrons (H 1s, Th 6s, 6p, 6d, and 7s) and Th 5s, 5p, and 5d core−shell electrons. The bond distances and frequencies were calculated using a seven-point Dunham expansion.[25,26] The diatomic potential energy functions were obtained by calculating seven single-point energies distributed around the approximate equilibrium bond length of their respective electronic states ($r - r_e$ = −0.3, −0.2, −0.1, 0.0, +0.1, +0.3, and +0.5 in Bohr). The CCSD(T) total energies were extrapolated to the CBS limit by fitting to a mixed Gaussian/exponential (eq 1)[27]

$$E(n) = E_{CBS} + A \exp[-(n-1)] + B \exp[-(n-1)^2] \quad (1)$$

with n = D through Q (n = 2, 3, and 4). The open-shell calculations were carried out with the R/UCCSD(T) approach, where a restricted open-shell Hartree−Fock calculation was initially performed and the spin constraint was then relaxed in the coupled-cluster calculation.[17,28−30] The CCSD(T) calculations were performed with the MOLPRO program package.[31,32] The calculations were performed on our local UA Opteron- and Xeon-based Linux clusters.

In order to interpret the observed photoelectron spectra, two series of calculations were performed. The first set involved calculations to ascertain the low-lying excited states of ThH^+, ThH, and ThH^-. These utilized the complete active-space self-consistent field (CASSCF) method together with second-order perturbation theory (CASPT2) and spin−orbit coupling via the state interaction approach. The second focused on a quantitative prediction of the ionization potential and EA of ThH using the composite Feller−Peterson−Dixon (FPD) methodology based on relativistic coupled-cluster methods. Both are described in detail in this section.

For all ThH species (neutral, anions, and cations), state-averaged CASSCF[33,34] calculations were performed to represent the lowest spin-free, ΛS, states, using the aug-cc-pV*n*Z basis sets[22,35] for H and the cc-pV*n*Z-PP basis sets with 60-electron small-core effective core potentials (abbreviated as PP) for Th,[24,36] for n = D, T, and Q. These basis sets are noted as a*n*-PP. These calculations were carried out in the highest abelian point group available, C_{2v}, for the ThH, ThH^-, and ThH^+ molecules. The expectation values of L_z^2, which ensure that both degenerate components of each Λ state were correctly accounted for, were calculated.

The relevant spin-free states (denoted as ΛS) that might contribute to the final relativistic |Ω| states of interest must be determined. To predict the relevant low-lying states, one can start with the lowest atomic asymptotes and investigate the molecular states that arise from coupling these. For all the studied species, ThH, ThH^-, and ThH^+, an ionic model was initially adopted; the H^- anion is treated as a closed shell in these couplings so that Th^+ (for ThH), Th^0 (for ThH^-), or Th^{2+} (for ThH^+) determine the resulting molecular states. Thus, for Th^+ ($6d^17s^2$), the low-lying states correspond to doublets and quartets; for Th ($6d^27s^2$), the low-lying states correspond to triplets and singlets; and for Th^{2+} ($6d^17s^1$ or $7s^2$), the low-lying states correspond to triplets and singlets. The same results arise if one chooses a model with a Th−H doubly occupied orbital. As discussed below, both configurations are likely to be present. Different CASSCF active spaces were tested with Th 6d, 7s, and 7p and H 1s orbitals included. Although this might be expected to involve a total of nine active orbitals, only eight were found to be strongly

https://doi.org/10.1021/acs.jpca.1c07598
J. Phys. Chem. A 2022, 126, 198−210

occupied and the orbital with dominant $6d_{z^2}$ character was omitted [although the molecular orbital (MO) with dominant $7p_z$ character is strongly mixed with $6d_{z^2}$]. We thus followed the approach used previously for the similar diatomic species, ThF and ThCl.[37−39] Hence, for ThH, three electrons in eight orbitals ($3 \times a_1$, $2 \times b_1$, $2 \times b_2$, and $1 \times a_2$), CASSCF (3/8), were included in the CASSCF active space, with all of the lower-energy orbitals constrained to be doubly occupied. The CASSCF active space for ThH^- included four electrons in the same effective eight orbitals giving a (4/8) CASSCF, and the CASSCF active space for ThH^+ included two electrons in the same effective eight orbitals giving a (2/8) CASSCF. In the end, doublet and quartet electronic states were calculated for ThH; triplet, quintet, and singlet electronic states were calculated for ThH^-; and triplet and singlet electronic states were calculated for ThH^+. For all three ThH species individually, the electronic states (ΛS states) were state-averaged to obtain a common set of orbitals.

Post-CASSCF calculations using the same active spaces as the preceding CASSCF calculations were carried out via second-order perturbation theory (CASPT2).[40,41] Thus, multiple states are calculated using a Fock operator constructed from a state-averaged density matrix and the zeroth-order Hamiltonians for all states. The frozen-core definition in the CASPT2 included all orbitals of Th through the 5d orbital (6s6p5f7s valence). The smallest possible IPEA shift[42] was used, a value of 0.28 for all states.

The state interaction method for the treatment of SO coupling,[43] implemented in MOLPRO, was used to calculate the molecular Ω states, SO-CASPT2. The spin−orbit eigenstates are obtained by diagonalizing $H_{el} + H_{SO}$ based on H_{el} eigenstates. The matrix elements of H_{SO} were constructed using the spin−orbit operator from the Th PP. Here, the spin−orbit matrix elements have been calculated throughout at the CASSCF level of the theory, whereas the diagonal terms of $H_{el} + H_{SO}$ have been replaced with CASPT2 energies. The latter energies for the two components of each molecular state with $\Lambda \neq 0$ were manually averaged when needed to ensure exact degeneracies. After diagonalization of $H_{el} + H_{SO}$, the values of Ω for each molecule were assigned by converting from a Cartesian eigenfunction basis to a spherical basis and then adding the projection of the spin angular momentum S on the diatomic axis, Σ, to Λ to obtain Ω. These calculations were performed using the a*n*-PP basis set at the corresponding optimized aw*n*-DK bond distances, for n = D, T, and Q.

To obtain benchmark FPD[44−47] values for the EA of ThH and its ionization energy (IE) and BDEs of all three species, additional calculations were performed. These included (a) higher-order correlation corrections beyond CCSD(T), (b) four-component treatments of spin−orbit coupling, and (c) quantum electrodynamics (QED) corrections for the Lamb shift. The (frozen-core) higher-order correlation corrections were calculated with the DKH3 Hamiltonian as ΔE_T = CCSDT − CCSD(T) in aT-DK basis sets[48,49] and as ΔE_Q = CCSDT(Q) − CCSDT in aD-DK basis sets.[50] These calculations utilized the MRCC program of Kállay and coworkers[51] interfaced to MOLPRO.

Effects due to spin−orbit coupling were calculated as the difference between calculations with the four-component Dirac−Coulomb (DC) or Dirac−Coulomb−Gaunt (DCG) Hamiltonians and analogous calculations with the spin-free Hamiltonian of Dyall.[52] These calculations were carried out with the DIRAC program[53] using fully uncontracted basis sets, cc-pVDZ-DK3 on Th and aug-cc-pVDZ on H, with a finite-nucleus model. For the open-shell species, spinors/orbitals were obtained from average-of-configuration Dirac−Hartree−Fock calculations (AoC-DHF) with an open-shell space defined by the Th 7s and four components of the 6d orbitals (the $6d_{z^2}$ is involved in the bond). For the $^1\Sigma^+$ state of ThH^+, frozen-core CCSD(T) calculations[54] were carried out, whereas for the $^3\Delta$ state, the (1,1) sector was utilized in intermediate Hamiltonian Fock-Space CCSD (IH-FS-CCSD) calculations.[55] In the latter case, the primary space involved the four 6d spinors with an auxiliary space defined by the spinors arising from the Th 7p and 5f orbitals with the orbitals being obtained from the $^1\Sigma^+$ state of ThH^+ as the (0,0) sector. Virtual orbital cutoffs of 12 a.u. were used for both sets of coupled-cluster calculations with the DCG Hamiltonian. It should be noted here that the modest auxiliary space and virtual orbital cutoffs would probably not be sufficient for calculating the spectrum of electronic states of ThH^+ but are more than sufficient to recover SO effects on the IE. For the remaining calculations, the SO corrections were obtained from Kramers-restricted configuration interaction (KRCI)[56] and scalar relativistic multireference CI (MRCI)[57,58] calculations with the DC Hamiltonian. Both of these approaches used a generalized active space (GAS) approach with four GAS spaces: (i) the 6s orbital which was constrained to be doubly occupied (but correlated), (ii) the 6p orbitals which were allowed minimum/maximum occupations of 4/6, (iii) six active valence orbitals with min/max occupations of 11/13 (ThH) and 12/14 (ThH^-), and (iv) virtual orbitals up to an orbital energy of 10 a.u. For these KRCI/MRCI cases, contributions from the Gaunt term were obtained as the difference between DHF calculations using the DCG and DC Hamiltonians, respectively.

Small effects due to the leading contribution of QED, the Lamb shift, were obtained using the local model potential approach proposed by Pyykkö and Zhao[59] for the self-energy term, including a fit to the Uehling potential for the vacuum polarization.[24] These calculations were carried out at the frozen-core DK3-CCSD(T) level of theory with awD-DK basis sets.

To obtain a better understanding of the bonding of these ThH species, the natural population analysis (NPA) results based on the natural bond orbitals (NBOs)[60,61] using NBO7[62,63] are calculated using the MOLPRO program package at the aD-DK level.

RESULTS AND DISCUSSION

Photoelectron Spectrum of ThH. The mass spectra of ThH_n^- and ThD_n^- are presented in Figure 1. When the Th rod was ablated in the presence of H_2 gas, the Th^-, ThH^-, ThH_2^-, and ThH_3^- anions were generated. Due to slight overlap between the Th^- and ThH^- anions, the experiment was repeated in the presence of D_2 gas. Photoelectron spectra were collected for the Th^-, ThH^-, and ThD^- anions (232, 233, and 234 amu, respectively).

The experimental PES spectrum for Th^- (Figure 2) is compared to the published results of Tang et al. (Table 1).[1] The experimental EA of Th (0.614 eV) is in excellent agreement with the high-resolution results of Tang et al. (0.607 eV). Other transitions, including those from the excited state of Th^-, are also in good agreement with the results of Tang et al.[1] Computationally, we obtain a value of 0.579 eV for the EA of Th at the CCSD(T)/CBS-DK level where no spin−orbit or

https://doi.org/10.1021/acs.jpca.1c07598
J. Phys. Chem. A 2022, 126, 198−210

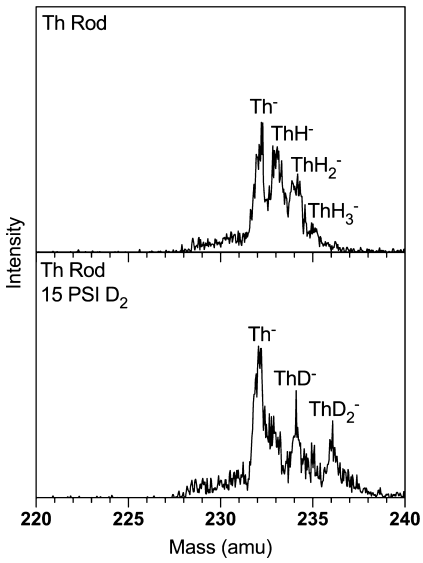

Figure 1. Mass spectra obtained using (a) no backing gas forming the anions Th^-, ThH^-, ThH_2^-, and ThH_3^- and (b) 15 psi of D_2 forming the anions Th^-, ThD^-, and ThD_2^-.

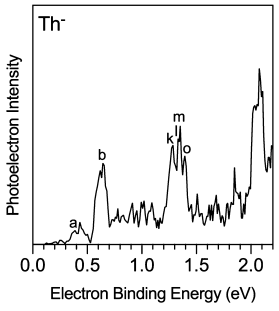

Figure 2. Photoelectron spectrum obtained using 532 nm photons to photodetach Th^-.

Table 1. Experimental EBEs of the Th^- Anion in eV

peak	current EBE	Tang et al.[1] EBE
a[a]	0.384	0.382
b[b]	0.614	0.607
k	1.286	1.298
l[a]	1.330	1.333
m[a]	1.347	1.339
o	1.394	1.397

[a]Photodetachment from excited states of Th^-. [b]Peak b corresponds to the EA of Th.

higher-order corrections are included. Peterson and co-workers obtained 0.565 eV for the EA of Th considering spin−orbit and higher-order corrections.[3]

The PES spectra of ThH^- and ThD^- are presented in Figure 3. The observed EBE peaks are given in Table 2. These transition energies are all fitted values with error bars of ±0.02 eV. The ThH^- PES spectrum is dominated by five peaks, while there are six prominent peaks in the ThD^- PES spectrum. Numerous additional weak peaks are present in both spectra.

Computational Assignment of Low-Lying Detachment Energies. To facilitate interpreting the complex PES spectra, calculations were performed on ThH^- and ThD^- to predict their low-lying states as shown in Tables 3 and 4 and for ThH in Tables 5 and 6. We first discuss the states of ThH^-

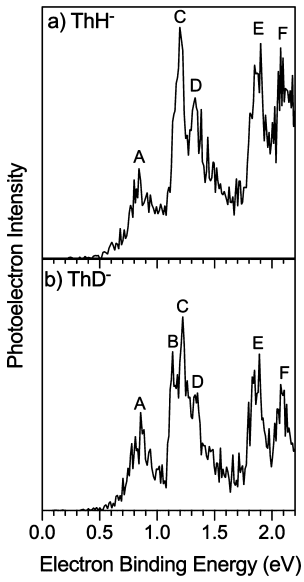

Figure 3. Photoelectron spectra of (a) ThH^- and (b) ThD^- obtained using the second harmonic (532 nm = 2.33 eV) of a Nd:YAG laser.

Table 2. EBEs in eV of the Observed Transitions Using 532 nm Photons to Photodetach the Anions ThH^- and ThD^-[a]

peaks	ThH^- EBE	ThD^- EBE
A (onset)	0.568	0.532
A (maxima)	0.868	0.859
B		1.137
C	1.205	1.227
D	1.332	1.326
E	1.890	1.893
F	2.080	2.079

[a]The EBE corresponds to the photoelectron intensity maxima of the transition unless otherwise noted.

to determine if there is a low-lying excited state that could be populated and interfere with the spectral assignments. The ground state for ThH^- is $^3\Phi_2$ with unpaired d_π and d_δ electrons. The first excited state for ThH^- is predicted to be the $^3\Sigma_0^-$ state, which is 0.121 eV higher in energy at the SO-CASPT2 level (Table 3) and 0.128 eV at the CCSD(T)/CBS level. The second excited state of ThH^- is predicted to be the $^3\Phi_3$ state, which is 0.244 eV above the ground state with a close-lying $^3\Sigma_1^-$ state that is 0.255 eV above the ground state of the anion at the CASPT2 level. The two triplet Σ^- states are highly mixed, whereas the two triplet Φ states are reasonably pure. The first singlet state is the $^1\Delta_2$ state which is 0.549 eV higher in energy, slightly below the $^3\Delta_1$ state at 0.588 eV. The spin−orbit correction to the ground state of ThH^- from the SO-CASPT2 calculation at the aQ-PP level using the awQ-DK-optimized geometry is 2090 cm^{-1} (0.259 eV). At the CCSD(T) level, different states were calculated to have similar bond distances and vibrational frequencies (Table 4).

At the SO-CASPT2 level, the ground state of ThH is predicted to be the $^2\Delta_{3/2}$ state with the first $^2\Pi_{1/2}$ state being only 0.043 eV (4.1 kJ/mol) higher in energy. In contrast, the CCSD(T) calculations predict the $^2\Pi$ state to be lower than the $^2\Delta$ by 0.011 eV, so the two states are almost degenerate at the CCSD(T) level without SO coupling included. The spin−orbit correction (lowering) to the ThH ground state ($^2\Delta_{3/2}$) from a SO-CASPT2 calculation with the aQ-PP basis set using

https://doi.org/10.1021/acs.jpca.1c07598
J. Phys. Chem. A 2022, 126, 198−210

Table 3. Low-Lying States of ThH^- at the CASPT2/aQ-PP + SO Level[a]

state	Ω	ΔE (eV)	ΓS composition
$^3\Phi_2$	2	0.000	92% $^3\Phi$ + 6% $^1\Delta$ + 3% $^3\Delta$
$^3\Sigma_0^-$	0	0.121	60% $^3\Sigma$ + 23% $^3\Pi$ + 17% $^1\Sigma$
$^3\Phi_3$	3	0.244	97% $^3\Phi$
$^3\Sigma_1^-$	1	0.255	58% $^3\Sigma^-$ + 34% $^3\Pi$ + 6% $^3\Delta$
$^3\Pi_0^+$ (1)	0	0.317	99% $^3\Pi$
$^3\Pi_0^+$ (2)	0	0.377	76% $^3\Pi$ + 15% $^3\Sigma$ + 7% $^1\Sigma$
$^3\Sigma_1^-$	1	0.387	38% $^3\Sigma^-$ + 36% $^3\Pi$ + 24% $^3\Delta$
$^3\Pi_2$	2	0.419	83% $^3\Pi$ + 8% $^1\Delta$ + 7% $^3\Delta$
$^3\Phi_4$	4	0.469	100% $^3\Phi$
$^1\Delta_2$	2	0.549	55% $^1\Delta$ + 35% $^3\Delta$ + 9% $^3\Phi$
$^3\Delta_1$	1	0.588	70% $^3\Delta$ + 26% $^3\Pi$
$^1\Sigma_0^+$	0	0.764	75% $^1\Sigma$ + 22% $^3\Sigma$
$^5\Pi_0^+$	0	0.779	61% $^5\Pi$ + 30% $^5\Sigma$ + 8% $^5\Delta$
$^5\Pi_1$ (1)	1	0.802	45% $^5\Pi$ + 29% $^5\Sigma$ + 21% $^5\Pi$
$^3\Delta_2$	2	0.819	53% $^3\Delta$ + 31% $^1\Delta$ + 14% $^3\Pi$
$^3\Delta_3$	3	0.829	94% $^3\Delta$ + 3% $^3\Phi$
$^5\Phi_0$	0	0.914	66% $^5\Phi$ + 39% $^5\Delta$
$^5\Pi_1$ (2)	1	0.933	40% $^5\Pi$ + 39% $^5\Pi$ + 16% $^5\Delta$
$^5\Pi_2$	2	0.939	54% $^5\Pi$ + 31% $^5\Sigma$ + 11% $^5\Delta$
$^5\Delta_0$	0	1.072	86% $^5\Delta$ + 13% $^5\Sigma$
$^5\Pi_3$	3	1.099	78% $^5\Pi$ + 18% $^5\Delta$
$^5\Delta_1$	1	1.119	46% $^5\Delta$ + 25% $^5\Phi$ + 10% $^5\Pi$
$^5\Delta_0$	0	1.126	69% $^5\Delta$ + 30% $^5\Pi$
$^5\Sigma_2^-$	2	1.152	46% $^5\Sigma$ + 39% $^5\Delta$ + 10% $^5\Phi$ + 4% $^5\Pi$
$^5\Sigma_1^-$	1	1.257	41% $^5\Sigma$ + 34% $^5\Phi$ + 23% $^5\Pi$
$^5\Pi_2$	2	1.276	36% $^5\Pi$ + 21% $^5\Sigma$ + 18% $^5\Delta$
$^5\Sigma_0^-$	0	1.285	55% $^5\Sigma$ + 37% $^5\Pi$ + 5% $^5\Delta$
$^5\Delta_3$	3	1.320	58% $^5\Delta$ + 22% $^5\Phi$ + 20% $^5\Pi$
$^5\Phi_1$	1	1.329	37% $^5\Phi$ + 24% $^5\Delta$ + 17% $^5\Pi$ + 11% $^5\Sigma$
$^5\Delta_4$	4	1.392	86% $^5\Delta$ + 13% $^5\Phi$
$^5\Phi_2$	2	1.453	65% $^5\Phi$ + 28% $^5\Delta$ + 4% $^5\Pi$

[a]Using the ThH^- ($^3\Phi$)-optimized CCSD(T)/awQ-DK geometry.

the CCSD(T)/awQ-DK-optimized geometry for the $^2\Delta$ state is 1534 cm^{-1} (0.190 eV). The spin–orbit correction to the ThH ground state ($^2\Delta_{3/2}$) from the SO-CASPT2 calculation at the aQ-PP level using the CCSD(T)/awQ-DK-optimized geometry for the $^2\Pi$ state, which is the lowest-energy state at the CCSD(T) level, is 1523 cm^{-1} (0.189 eV), so there is little dependence on these geometries. The energetics of the low-lying states for ThH at the CASPT2/aQ-PP + SO level using the ThH ($^2\Pi$)-optimized CCSD(T)/awQ-DK geometry are reported in the Supporting Information, and there are no significant changes in the state energies.

The inclusion of the spin–orbit correction is important in determining the ground state and switches the order from that obtained at the (spin-free) CCSD(T) level. The ground state of ThH at the SO-CASPT2 level consists of 68% $^2\Delta$ and 30% $^2\Pi$, whereas the first excited state is 91% $^2\Pi$. We note that ThF has a $^2\Delta_{3/2}$ ground state and that ThCl has a mixed $^2\Pi$ and $^2\Delta_{3/2}$ ground state, with the latter being similar to the ground state of ThH.[37,38] The vibrational frequency for ThH has been measured in Ne and Ar matrices[6] with respective values of 1511.0 and 1485.2 cm^{-1}. Our CCSD(T)/awQ-DK value for ThH for the $^2\Pi$ state (lowest at the CCSD(T) level) is 1530 cm^{-1} and for the $^2\Delta$ state (lowest at the CASPT2) is 1537 cm^{-1}; both are consistent with the experimental Ne value. A B3LYP value of 1494 cm^{-1} was reported for an unspecified electronic state and is clearly too low for the ground state. Our value at the B3LYP level for the lowest doublet state is 1531 cm^{-1} and for the lowest energy quartet is 1495 cm^{-1}.

We first discuss assignments of the PES from the ground state of the anion to excited states of neutral ThH. The components needed to calculate the electron detachment energies are given in Table 7. The adiabatic EA (AEA) is calculated to be 0.820 eV as shown in Table 7. To calculate the AEA, we used the $^2\Delta_{3/2}$ state of ThH and the $^3\Phi_2$ state of ThH^-. Note that this value above includes additional contributions including the Gaunt contribution and higher-order correlation effects. If we use the SO correction from the CASPT2 calculations, we obtain AEA = 0.804 eV. At the CCSD(T)/CBS level without additional corrections, the VDE is calculated to be 0.707 eV for the $^2\Delta$ state in the ThH^- ($^3\Phi$) geometry in comparison to a CCSD(T)/CBS adiabatic value of 0.680 eV; thus, the VDE is greater than the adiabatic EA by only 0.027 eV. We add 0.027 eV to the adiabatic value of 0.805 eV, which excludes the ΔZPE to obtain an estimate of the VDE of 0.832 eV. The calculated vertical and adiabatic EA values are consistent with peaks in the experimental PES

Table 4. Spectroscopic Properties of Low-Lying States of ThH^- at the CCSD(T) Level

ΛS state	basis set	T_e (eV)	T_e (cm^{-1})	r_e (Å)	B_e (cm^{-1})	ω_e (cm^{-1})	$\omega_e x_e$ (cm^{-1})
$^3\Phi$	awD-DK	0.0	0	2.120	3.738	1304.8	28.0
	awT-DK	0.0	0	2.108	3.781	1305.9	19.2
	awQ-DK	0.0	0	2.102	3.803	1321.8	18.3
	CBS	0.0	0				
$^3\Sigma^-$	awD-DK	0.131	1053	2.103	3.798	1309.9	26.4
	awT-DK	0.126	1014	2.088	3.853	1314.2	16.4
	awQ-DK	0.127	1023	2.083	3.873	1325.5	15.3
	CBS	0.128	1030				
$^3\Pi$	awD-DK	0.280	2260	2.143	3.658	1255.0	25.8
	awT-DK	0.294	2374	2.130	3.704	1255.1	22.2
	awQ-DK	0.308	2485	2.124	3.724	1264.4	25.9
	CBS	0.319	2575				
$^1\Delta$	awD-DK	0.553	4464	2.099	3.812	1323.2	23.6
	awT-DK	0.519	4189	2.082	3.877	1331.7	19.2
	awQ-DK	0.507	4089	2.074	3.905	1349.2	26.0
	CBS	0.500	4031				

https://doi.org/10.1021/acs.jpca.1c07598
J. Phys. Chem. A 2022, 126, 198–210

Table 5. Low-Lying States of ThH at the CASPT2/aQ-PP + SO Level[a]

state	Ω	eV	ΓS composition
$^2\Delta_{3/2}$ (1)	3/2	0.000	68% $^2\Delta$ + 30% $^2\Pi$
$^2\Pi_{1/2}$ (1)	1/2	0.043	91% $^2\Pi$ + 3% $^2\Sigma$ + 3% $^4\Pi$
$^4\Phi_{3/2}$	3/2	0.223	95% $^4\Phi$ + 4% $^2\Delta$
$^2\Pi_{3/2}$ (1)	3/2	0.339	60% $^2\Pi$ + 31% $^2\Delta$ + 4% $^4\Pi$ + 4% $^4\Sigma$
$^4\Sigma^-_{1/2}$ (1)	1/2	0.351	64% $^4\Sigma$ + 28% $^4\Pi$ + 4% $^2\Sigma$ + 3% $^2\Pi$
$^2\Delta_{5/2}$ (1)	5/2	0.407	59% $^2\Delta$ + 36% $^4\Phi$
$^4\Phi_{5/2}$	5/2	0.438	59% $^4\Phi$ + 38% $^2\Delta$
$^4\Sigma^-_{3/2}$(1)	3/2	0.488	77% $^4\Sigma$ + 16% $^4\Pi$ + 5% $^2\Pi$
$^4\Phi_{7/2}$	7/2	0.626	97 $^4\Phi$
$^4\Pi_{1/2}$ (1)	1/2	0.669	47% $^4\Pi$ + 45% $^4\Pi$ + 3% $^2\Pi$
$^4\Pi_{1/2}$ (2)	1/2	0.773	34% $^4\Pi$ + 30% $^4\Sigma$ + 23% $^4\Pi$ + 8% $^2\Pi$ + 2% $^2\Sigma$ + 2% $^4\Delta$
$^4\Pi_{3/2}$	3/2	0.780	70% $^4\Pi$ + 18% $^4\Sigma$ + 7% $^2\Pi$ + 3% $^4\Delta$ + 2% $^4\Sigma$
$^4\Pi_{5/2}$	5/2	0.799	94% $^4\Pi$ + 2% $^2\Delta$ + 2% $^4\Delta$
$^4\Phi_{9/2}$	9/2	0.805	94% $^4\Phi$ + 5% $^2\Gamma$
$^2\Phi_{5/2}$	5/2	1.079	96% $^2\Phi$ + 2% $^4\Phi$
$^2\Pi_{1/2}$ (2)	1/2	1.080	47% $^2\Pi$ + 41% $^2\Sigma$ + 7% $^4\Pi$ + 2% $^2\Pi$
$^4\Sigma^-_{3/2}$ (2)	3/2	1.179	94% $^4\Sigma$ + 3% $^4\Pi$
$^4\Sigma^-_{1/2}$ (2)	1/2	1.182	90% $^4\Sigma$ + 4% $^4\Pi$ + 2% $^4\Pi$ + 2% $^4\Sigma$
$^2\Sigma^+_{1/2}$ (1)	1/2	1.229	53% $^2\Sigma$ + 30% $^2\Pi$ + 7% $^4\Sigma$ + 6% $^4\Delta$ + 4% $^4\Pi$
$^2\Phi_{7/2}$	7/2	1.260	56% $^2\Phi$ + 42% $^2\Gamma$
$^2\Gamma_{9/2}$	9/2	1.464	94% $^2\Gamma$ + 5% $^4\Phi$
$^2\Pi_{3/2}$ (2)	3/2	1.501	79% $^2\Pi$ + 7% $^4\Delta$ + 5% $^4\Pi$ + 4% $^2\Delta$ + 3% $^4\Sigma$ + 2% $^2\Pi$
$^2\Gamma_{7/2}$	7/2	1.513	57% $^2\Gamma$ + 40% $^2\Phi$ + 2% $^4\Phi$
$^4\Delta_{1/2}$	1/2	1.530	85% $^4\Delta$ + 7% $^2\Pi$ + 4% $^2\Sigma$ + 2% $^4\Pi$
$^2\Delta_{3/2}$ (2)	3/2	1.538	63% $^2\Delta$ + 32% $^4\Delta$ + 4% $^4\Phi$
$^2\Sigma^+_{1/2}$ (2)	1/2	1.592	92% $^2\Sigma$ + 3% $^4\Sigma$ + 3% $^4\Delta$
$^2\Delta_{5/2}$ (2)	5/2	1.667	54% $^2\Delta$ + 41% $^4\Delta$ + 2% $^4\Phi$ + 2% $^2\Phi$
$^4\Delta_{3/2}$	3/2	1.713	56% $^4\Delta$ + 29% $^2\Delta$ + 13% $^2\Pi$
$^2\Sigma^-_{1/2}$	1/2	1.808	91% $^2\Sigma$ + 6% $^2\Sigma$
$^4\Delta_{5/2}$	5/2	1.817	55% $^4\Delta$ + 42% $^2\Delta$ + 3% $^4\Pi$
$^4\Delta_{7/2}$	7/2	1.855	94% $^4\Delta$ + 3% $^2\Phi$

[a]In the ThH ($^2\Delta$)-optimized CCSD(T)/awQ-DK geometry.

Table 6. Spectroscopic Properties of Low-Lying States for ThH at the CCSD(T) Level

ΛS state	basis set	T_e (eV)	T_e (cm^{-1})	r_e (Å)	B_e (cm^{-1})	ω_e (cm^{-1})	$\omega_e x_e$ (cm^{-1})
$^2\Pi$	awD-DK	0.0	0	2.015	4.136	1557.3	20.7
	awT-DK	0.0	0	2.008	4.164	1546.7	20.0
	awQ-DK	0.0	0	2.006	4.175	1559.3	14.3
	CBS	0.0	0				
$^2\Delta$	awD-DK	0.013	107	2.027	4.087	1564.3	20.1
	awT-DK	0.011	92	2.023	4.105	1549.9	18.7
	awQ-DK	0.011	89	2.020	4.117	1557.2	19.9
	CBS	0.011	87				
$^4\Phi$	awD-DK	0.492	3969	2.063	3.946	1487.4	19.4
	awT-DK	0.462	3727	2.055	3.977	1480.6	18.4
	awQ-DK	0.447	3607	2.052	3.990	1487.5	24.2
	CBS	0.438	3534				
$^4\Sigma^-$	awD-DK	0.796	6421	2.051	3.994	1476.4	17.8
	awT-DK	0.756	6099	2.039	4.039	1476.0	20.3
	awQ-DK	0.740	5966	2.035	4.055	1483.9	18.7
	CBS	0.730	5888				
$^2\Sigma^+$	awD-DK	0.861	6946	2.093	3.835	1434.0	20.3
	awT-DK	0.830	6696	2.088	3.854	1419.8	18.7
	awQ-DK	0.806	6502	2.082	3.874	1436.4	18.9
	CBS	0.791	6379				

spectra of ThH^- and ThD^- just before the first large maximum in the PES spectrum at 0.868 eV for ThH^- and at 0.859 eV for ThD^-. The first excited state (Table 8) of ThH with a VDE of 0.873 eV is right at the first maximum in the PES spectrum.

https://doi.org/10.1021/acs.jpca.1c07598
J. Phys. Chem. A 2022, 126, 198−210

Table 7. FPD Components for the EA and IE of ThH in eV

property	neutral	ion	awD-DK	awT-DK	awQ-DK	ΔE_{CBS}[a]	$\Delta E_{SO+Gaunt}$[b]	ΔE_{QED}[c]	ΔE_T[d]	ΔE_Q[e]	ΔE_{ZPE}[f]	final (0 K)
AEA	ThH ($^2\Delta_{3/2}$)	ThH^- ($^3\Phi_2$)	0.515	0.607	0.644	0.680	0.085 (0.069)[h]	0.011	0.005	0.024	0.015	0.820 (0.804)[h]
VDE[g]			0.563	0.650	0.686	0.707						0.832[i]
IE	ThH ($^2\Delta_{3/2}$)	ThH^+ ($^3\Delta_1$)	6.105	6.133	6.150	6.161	−0.024 (−0.046)[h]	−0.011	0.020	0.027	0.008	6.181 (6.159)[h]

[a]CCSD(T) value extrapolated to the CBS limit using awn-DK basis sets for n = D, T, and Q. [b]Using KRCI/MRCI for the EA and IH-FS-CCSD for the IE. Both include a DHF Gaunt contribution. [c]Correction for the Lamb shift. [d]ΔE_T = CCSDT − CCSD(T). [e]ΔE_Q = CCSDTQ − CCSDT. [f]CCSD(T)/awQ-DK. [g]ThH ($^2\Delta_{3/2}$) at ThH^- ($^3\Phi_2$) geometry for each level of theory. [h]SO-CASPT2 values: ThH^- = 0.259 eV (2090 cm^{-1}), ThH = 0.190 eV (1534 cm^{-1}), and ThH^+ = 0.144 eV (1164 cm^{-1}). [i]value does not include a ZPE correction but includes the same other corrections as calculated for the AEA.

Table 8. Calculated VDEs at the CASPT2/aQ-PP + SO Level[a]

state	VDE
$^2\Delta_{3/2}$ (1)	0.832
$^2\Pi_{1/2}$ (1)	0.873
$^4\Phi_{3/2}$	1.026
$^2\Pi_{3/2}$ (1)	1.156
$^4\Sigma_{1/2}^-$ (1)	1.172
$^2\Delta_{5/2}$ (1)	1.219
$^4\Phi_{5/2}$	1.264
$^4\Sigma_{3/2}^-$ (1)	1.298
$^4\Phi_{7/2}$	1.435
$^4\Pi_{1/2}$ (1)	1.475
$^4\Pi_{1/2}$ (2)	1.578
$^4\Pi_{3/2}$	1.585
$^4\Pi_{5/2}$	1.606
$^4\Phi_{9/2}$	1.618
$^2\Phi_{5/2}$	1.880
$^2\Pi_{1/2}$ (2)	1.891
$^4\Sigma_{3/2}^-$ (2)	1.984
$^4\Sigma_{1/2}^-$ (2)	2.003
$^2\Sigma_{1/2}^+$ (1)	2.008
$^2\Phi_{7/2}$	2.071
$^2\Gamma_{9/2}$	2.271
$^2\Pi_{3/2}$ (2)	2.274
$^2\Gamma_{7/2}$	2.275
$^4\Delta_{1/2}$	2.304
$^2\Delta_{3/2}$ (2)	2.320
$^2\Sigma_{1/2}^+$ (2)	2.392
$^2\Delta_{5/2}$ (2)	2.432
$^4\Delta_{3/2}$	2.472
$^2\Sigma_{1/2}^-$	2.583
$^4\Delta_{5/2}$	2.603
$^4\Delta_{7/2}$	2.639

[a]In the optimized ThH^- ($^3\Phi$) CCSD(T)/awQ-DK geometry.

However, these values from the ground state of the anion do not account for the observed tail to lower EBE. The tail goes down to almost 0.50 eV. In this case, there may be some Th^- present as this is in the region of the adiabatic EA for Th. We should also consider electron detachment from the first two excited states of ThH^-. These are the $^3\Sigma_0^-$ and $^3\Phi_3$ states, which are 0.121 and 0.244 eV, respectively, higher in energy than the ground state of ThH^- at the CASPT2 level. Subtracting these from the VDE value of 0.832 eV gives detachment from these states at 0.711 and 0.588 eV, respectively. The intensity of peaks below the VDE suggests the presence of excited states in ThH^- contributing to the spectrum and the possibility of Th^- noted above. In addition, we should note that detachment from excited vibrational levels of the anion could also contribute to the lower values of the detachment energies as the first vibrational state of the anion is located at 1325 cm^{-1} (0.164 eV).

We now return to describe the excited states of ThH and potential assignments of various EBEs in the PES spectrum. The second excited state of ThH is the $^4\Phi_{3/2}$ state with a predicted VDE of 1.026 eV, consistent with intensity in the valley between the A and B maxima (Table 2, Figure 3). The calculated energies at 1.516 and 1.172 eV for the $^2\Pi_{3/2}$ and $^4\Sigma_{1/2}^-$ states, respectively, are consistent with the EBE of 1.127 eV in the ThD^- spectrum. The $^2\Delta_{5/2}$ state is predicted to be at 1.219 eV, consistent with the experimental EBEs of 1.205 and 1.227 eV for ThH^- and ThD^-, respectively. The $^4\Sigma_{3/2}^-$ state with a predicted VDE of 1.298 eV is consistent with the observed EBEs of 1.332 and 1.326 eV for ThH^- and ThD^-, respectively. The $^4\Phi_{5/2}$ state falls between the $^2\Delta_{5/2}$ state and the $^4\Sigma_{3/2}^-$ state at 1.264 eV.

The next intense experimental peak has an EBE of 1.890 and 1.893 eV for ThH^- and ThD^-, respectively (Figure 3). In between these peaks and the experimental ones near 1.33 eV are six predicted excited states for ThH ranging from 1.435 to 1.618 eV, consistent with the intensity observed in this region. The calculated VDEs for the $^2\Phi_{5/2}$ and $^2\Pi_{1/2}$ states at 1.880 and 1.891 eV, respectively, are consistent with the experimental EBEs near 1.89 eV. The experimental EBEs of 2.080 and 2.079 eV for ThH^- and ThD^-, respectively, are consistent with the calculated value of 2.071 eV for the $^2\Phi_{7/2}$ state. Note that there are two additional transitions predicted between 1.89 and 2.08 eV. There are additional 11 VDEs predicted between 2.25 and 2.65 eV.

Calculated Properties of ThH^+. The IE of ThH is calculated at the FPD level to be 6.181 eV as shown in Table 7 from the $^2\Delta_{3/2}$ state of ThH to the $^3\Delta_1$ state of ThH^+. If we use the spin−orbit correction of 0.046 eV from the SO-CASPT2 calculations, the predicted IE is 6.159 eV. Using the computational data obtained at the same level as the current work from ref 10, the IE of Th is calculated to be 6.281 eV in excellent agreement with the experimental value of 6.30670 ± 0.00025 eV.[64] The calculated IE of ThH is 0.10 eV lower than the calculated IE for Th. As the IE of ThH and Th atom is very similar, we suggest that the H^- remains unchanged as a ligand on ionization, implying that ThH has a significant Th^+H^- ionic component.

The low-lying states predicted for ThH^+ are shown in Tables 9 and 10. At the SO-CASPT2 level, the ground state of ThH^+ is predicted to be the $^3\Delta_1$ state with the first $^1\Sigma_0^+$ excited state only 0.027 eV (2.6 kJ/mol) higher in energy. In contrast, the (scalar relativistic) CCSD(T) calculations predict the $^1\Sigma^+$ state to be lower than the $^3\Delta$ state by 0.030 eV, so the two states are

https://doi.org/10.1021/acs.jpca.1c07598
J. Phys. Chem. A 2022, 126, 198−210

Table 9. Low-Lying States of ThH^+ at the CASPT2/aQ-PP + SO Level[a]

state	Ω	ΔE (eV)	ΓS composition
$^3\Delta_1$	1	0.000	92% $^3\Delta$ + 7% $^3\Pi$
$^1\Sigma_0^+$	0	0.027	78% $^1\Sigma^+$ + 17% $^3\Pi$ + 4% $^3\Sigma^-$
$^3\Delta_2$	2	0.157	86% $^3\Delta$ + 9% $^3\Pi$ + 2% $^3\Delta$
$^3\Delta_3$	3	0.446	96% $^3\Delta$ + 4% $^3\Phi$
$^3\Pi_0$	0	0.487	100% $^3\Pi$
$^3\Pi_0$	0	0.539	76% $^3\Pi$ + 20% $^1\Sigma^+$ + 3% $^3\Sigma^-$
$^3\Phi_2$	2	0.550	94% $^3\Phi$
$^3\Pi_1$	1	0.604	83% $^3\Pi$ + 10% $^3\Sigma^-$ + 4% $^3\Delta$
$^3\Pi_2$	2	0.756	88% $^3\Pi$ + 11% $^3\Delta$
$^3\Phi_3$	3	0.869	96% $^3\Phi$
$^3\Sigma_1$	1	0.928	90% $^3\Sigma^-$ + 9% $^3\Pi$
$^3\Sigma_0^-$	0	0.947	93% $^3\Sigma^-$ + 69% $^3\Pi$
$^3\Phi_4$	4	1.166	80% $^3\Phi$ + 20% $^3\Phi$
$^1\Delta_2$	2	1.284	96% $^1\Delta$ + 3% $^3\Delta$

[a]In the ThH^+ ($^3\Delta$)-optimized CCSD(T)/awQ-DK geometry.

still close in energy at the CCSD(T) level. The spin−orbit lowering (from SO-CASPT2) of the $^3\Delta_1$ state is 1164 cm^{-1} (0.144 eV). Thus, by including spin−orbit coupling, the ground state switches the order from what was obtained at the (scalar relativistic) CCSD(T) level. The spin−orbit correction to the ThH^+ ground state ($^3\Delta$) from the SO-CASPT2 calculation at the aQ-PP level using the $^1\Sigma^+$ ThH^+ awQ-DK-optimized geometry (the lowest energy state at the CCSD(T) level) is 1116 cm^{-1} (0.138 eV), and these ThH^+ low-lying states are given in the Supporting Information. The $^2\Delta_1$ ground state of ThH^+ at the CASPT2 level consists of 92% $^3\Delta$, and the first excited state is 78% $^1\Sigma^+$ and 17% $^3\Sigma^-$.

The above results on the role of spin−orbit in the states of ThH^+ are consistent with the results of Armentrout and co-workers using a semi-empirical spin−orbit correction.[4] These authors predict the $^3\Delta_1$ state to be the ground state by 0.13 eV when an empirical spin−orbit correction is used and the $^1\Sigma_0^+$ state to be the ground state at the CCSD(T) level with a quadruple zeta correlation-consistent basis set by 0.05 eV. The CCSD(T) bond distances are in agreement with our values within 0.01 Å.

Thermochemistry. The BDEs for ThH, ThH^-, and ThH^+ at 0 K were calculated to provide additional insights into the bonding. The FPD composite energy values are given in Table 11. We dissociate the diatomics to a Th atom plus $H^{0/+/-}$ for consistency and because it is more difficult to calculate the absolute energy of the Th^+ atom. This will give the lowest BDE except for ThH^+ which will dissociate into Th^+ and H. We correct the BDE for ThH^+ to the Th^+ + H asymptote by the difference in the experimental ionization energies for Th and H, which are well established as 13.59843 eV for H[65] and 6.30670 ± 0.00025 eV for Th.[64] The BDEs for the most stable species are 259.0 kJ/mol (2.684 eV) for ThH, 278.7 kJ/mol (2.888 eV) for ThH^-, and 272.0 (2.819 eV) kJ/mol for ThH^+. Thus, the BDEs are all quite similar.

The spin−orbit corrections to the BDEs cannot be neglected. In all cases except for ThH^-, the atomic spin−orbit correction of approximately 37 kJ/mol for the Th atom is partially quenched. The $^2\Pi_{1/2}$ state of ThH has very little spin−orbit so the atomic spin−orbit correction is not quenched, leading to a decrease in the BDE. In contrast, the SO correction for the $^2\Delta_{3/2}$ state of ThH is about 21 kJ/mol and the atomic spin−orbit is partially quenched, making the $^2\Delta_{3/2}$ state the lowest energy state. For ThH^+, a similar difference in quenching for the lowest-lying states occurs with more spin−orbit quenching in the $^3\Delta_1$ state, so it is the ground state. Surprisingly, the spin−orbit effects for ThH^- are such that the overall correction to the BDE is only slightly negative. The QED corrections are all quite small but are not inconsequential. The full CCSDT and CCSDTQ corrections can have different signs. For the $^1\Sigma_0^+$ state of ThH^+, the full T and Q corrections increase the BDE with only a small contribution from the Q. For the $^3\Delta_1$ state of ThH^+, the full T and Q corrections decrease the BDE and the Q correction is larger than the T correction. This brings the two states closer together. The corrections for ThH are smaller with the $^2\Pi_{1/2}$ state being stabilized, and there is essentially no impact on the $^2\Delta_{3/2}$ state. The T and Q corrections also increase the BDE of ThH^-.

Our value for the BDE of ThH^+ of 2.819 eV confirms the prior CCSD(T) computational work of Armentrout and co-workers,[4] who predicted a value of 2.72 eV using lower-level calculations. The current results suggest that their experimentally derived value of 2.45 ± 0.07 eV may be too low. We do not know what has led to this difference between theory and experiments for this diatomic hydride. We do note that our calculated BDE for ThH^+ uses the same levels of theory that previously predicted the BDEs of other small molecules containing thorium to be better than 0.13 eV (12 kJ/mol),[8−11] an error estimate far smaller than the difference of almost 0.4 eV.

Table 10. Spectroscopic Properties of Low-Lying States for ThH^+ at the CCSD(T) Level

ΛS state	basis set	T_e (eV)	T_e (cm^{-1})	r_e (Å)	B_e (cm^{-1})	ω_e (cm^{-1})	$\omega_e x_e$ (cm^{-1})
$^1\Sigma^+$	awD-DK	0.00	0	1.958	4.381	1736.6	23.2
	awT-DK	0.00	0	1.959	4.377	1712.8	21.7
	awQ-DK	0.00	0	1.958	4.384	1727.6	22.4
	CBS	0.00	0				
$^3\Delta$	awD-DK	0.094	757	1.990	4.242	1692.8	21.0
	awT-DK	0.066	536	1.988	4.249	1674.3	18.8
	awQ-DK	0.044	355	1.986	4.258	1677.5	20.3
	CBS	0.030	240				
$^3\Pi$	awD-DK	0.419	3382	1.976	4.300	1682.0	23.0
	awT-DK	0.367	2961	1.974	4.313	1657.5	15.7
	awQ-DK	0.335	2699	1.973	4.317	1667.0	23.6
	CBS	0.315	2537				

https://doi.org/10.1021/acs.jpca.1c07598
J. Phys. Chem. A 2022, 126, 198−210

Table 11. FPD Components for BDEs in kJ/mol

ThH^x	state	ΔE_{CBS}[a]	$\Delta E_{SO+Gaunt}$	ΔE_{QED}[b]	ΔE_T[c]	ΔE_Q[d]	ΔE_{ZPE}[e]	D_0
ThH$^+$	$^1\Sigma_0^+$	1002.6	−30.3[f]	−0.6	4.3	0.2	−10.2	966.0
ThH$^+$	$^3\Delta_1$	999.8	−10.8[g]	1.0	−1.6	−3.1	−10.0	975.3
ThH	$^2\Pi_{1/2}$	282.5	−22.5[h]	0.2	2.3	0.5	−9.2	253.8
ThH	$^2\Delta_{3/2}$	281.4	−11.6[h]	0.1	0.3	−0.5	−9.2	260.5
ThH$^-$	$^3\Phi_2$	274.5	−3.4[h]	1.1	0.8	1.9	−7.9	267.0

[a]CCSD(T) value extrapolated to the CBS limit using awn-DK basis sets for n = D, T, and Q. [b]Correction for the Lamb shift. [c]ΔE_T = CCSDT − CCSD(T). [d]ΔE_Q = CCSDTQ − CCSDT. [e]CCSD(T)/awQ-DK. [f]Using 4c-CCSD(T) and the DCG Hamiltonian. The 4c-CCSD value is −25.6 kJ/mol. [g]Using 4c-IH-FS-CCSD and the DCG Hamiltonian. [h]Using 4c-KRCI/MRCI with a DHF Gaunt contribution.

Given the BDEs, we can calculate the heats of formation of ThH$^{0/-/+}$ from the known atomic heats of formation of ΔH_f^0 (0 K, Th) = 602.1 ± 6 kJ/mol,[66] ΔH_f^0 (0 K, H) = 216.034 kJ/mol, ΔH_f^0 (0 K, H$^+$) = 1528.084 kJ/mol, and ΔH_f^0 (0 K, H$^-$) = 143.264 kJ/mol from the active thermochemical tables.[65,67,68] The heats of formation are given in Table 12,

Table 12. Heats of Formation (ΔH_f^0) of ThH$^{0/-/+}$ in kJ/mol at 0 and 298 K

diatomic	ΔH_f^0 (0 K)	ΔH_f^0 (298 K)
ThH	557.7	553.1
ThH$^-$	478.2	474.0
ThH$^+$	1154.8	1150.2

and we estimate an error bar of ±8 kJ/mol with most of the error from the error in ΔH_f^0 (0 K, Th). Heats of formation at 298 K were calculated following the procedures outlined by Curtiss et al.[69] using 6.49 kJ/mol for the thermal corrections for Th[70] and 4.23 kJ/mol for the thermal corrections for H.

Electronic Structure Analysis. Inspection of the MO coefficients of ThH and ThH$^+$ reveals that each can be considered as arising from a mixture of ionic and covalent interactions, for example, for ThH, the low-lying states arise from the 7s^{2}6d^2 state of Th bonding with the 1s electron of H and the 7s^{2}6d^1 state of Th$^+$ with the closed-shell 1s^2 state of H$^-$. For ThH, the highest occupied MO of σ symmetry closely corresponds to a Th 7s orbital whereas the next lowest σ orbital is a bonding orbital strongly polarized toward H. If one considers the low-lying states of ThH as being derived from the 7s^{2}6d^2 state of the atom, the electron in the 1s orbital on H interacts with a 6d orbital along the molecular axis giving rise to a $^2\Pi$ or $^2\Delta$ state depending on which 6d orbital the lone electron on Th occupies. In fact, there are two such low-lying states within 0.011 eV of each other at the CCSD(T)/CBS level that split apart due to spin−orbit effects. The SO-CASPT2 calculations show that the ground state is a mixture of these states.

For ThH$^-$, one can derive the states by adding H$^-$ to Th as the Th EA is lower than that of H. The character of the MOs also supports this interpretation. The interaction of Th with H$^-$ would give rise to $^3\Phi$, $^3\Sigma^-$, and $^3\Pi$ depending on the distribution of the two unpaired 6d electrons on the Th. Hence, the two highest occupied σ orbitals qualitatively correspond to doubly occupied 7s (Th) and 1s (H) orbitals.

The ground state for ThH$^-$ is the $^3\Phi$ state with the $^3\Sigma^-$ state being 0.128 eV higher in energy at the CCSD(T)/CBS level. For ThH$^+$, the bonding can be described as the interaction of H with Th$^+$ as the IE for Th is much lower than that for H. The ground state for Th$^+$ is complicated as it is a mixture of 7s^{2}6d^1 (^{2}D) and 7s^{1}6d^2 (^{4}F). If the H interacts with the 6d orbital in the ^{2}D state, then one obtains the $^1\Sigma_0^+$ state. If the H interacts with the ^{4}F state, then one can obtain a variety of states including a $^3\Delta$ state, where the H 1s interacts with the 7s^1 electron leaving two unpaired electrons on Th. Of course, as noted above, these states can also be interpreted as arising from states of Th^{+2} (7s^2 or 7s^{1}6d^1) interacting with H$^-$. At the CCSD(T)/CBS level, the $^3\Delta$ state is 0.029 eV above the $^1\Sigma^+$ state at the CCSD(T)/CBS level. Spin−orbit and higher-order correlation effects make the $^3\Delta$ state the ground state by 0.094 eV.

The NPA charges from the NBO analysis are consistent with this discussion of the bonding (Table 13). For ThH, there are about 0.6e additional electrons on the H (Th$^{0.6}$H$^{-0.6}$), consistent with the Th$^+$H$^-$ ionic configuration being important. The Th 7s is doubly occupied with ∼1.8e in the 7s.

The remaining Th electron density is predominan in the 6d orbital with the unpaired spin in the 6d and about 0.5e in doubly occupied 6d character. There are small 5f and 7p populations.

For ThH$^-$, the charge difference between the Th and H$^-$ decreases to 0.4e from a difference of almost 1.2e between Th

Table 13. NBO/HF Charges (q) and Th Population at aD-DK Level from MOLPRO[a]

	q(Th)	q(H)	5f	6d	7s	7p	H 1s
				ThH			
$^2\Pi_{1/2}$	0.585	−0.585	0.08 (0.06/0.02)	1.50 (1.22/0.28)	1.81 (0.90/0.90)	0.04 (0.03/0.01)	1.57 (0.78/0.78)
$^2\Delta_{3/2}$	0.598	−0.598	0.04 (0.02/0.02)	1.48 (1.24/0.24)	1.86 (0.93/0.93)	0.04 (0.02/0.02)	1.58 (0.79/0.79)
				ThH$^-$			
$^3\Phi_2$	−0.297	−0.703	0.03 (0.02/0.01)	2.22 (2.04/0.18)	1.87 (0.94/0.94)	0.18 (0.15/0.03)	1.67 (0.84/0.84)
$^3\Sigma_0^-$	−0.305	−0.695	0.04 (0.02/0.01)	2.24 (2.04/0.20)	1.86 (0.93/0.93)	0.18 (0.16/0.02)	1.67 (0.83/0.83)
				ThH$^+$			
$^1\Sigma_0^+$	1.487	−0.487	0.06	0.73	1.73	0.01	1.46
$^3\Delta_1$	1.520	−0.520	0.06 (0.04/0.02)	1.55 (1.39/0.16)	0.89 (0.82/0.07)		1.50 (0.75/0.75)

[a]Values in parentheses are (α spin/β spin).

https://doi.org/10.1021/acs.jpca.1c07598
J. Phys. Chem. A 2022, 126, 198−210

and H in ThH. Most of the additional negative charge goes to the Th as the H^- only gains 0.1*e*. The Th 7s orbital remains doubly occupied with about 1.9*e*, and there are essentially two unpaired 6d electrons on the Th with a small amount of doubly occupied 6d character. There is no gain of electron density in the 5f and the 7p orbitals in the anion. Thus, an important electron configuration in the anion is Th^0H^-.

The charges for the cation, ThH^+, show that most of the electron density is removed from the Th with the H only losing ~0.1*e*. For the $^3\Delta_1$ state of ThH^+, the electron is removed from the Th 7s, leaving about 0.8 unpaired electrons in the 7s and 1.2 unpaired electrons in the 6d. The Th 6d population is comparable to that in the neutral. For the $^1\Sigma_0^+$ state, the lone electron on the Th 6d is removed and there is also loss of density from the Th 7s. These results are similar to what has been reported previously in terms of the Th orbital contributions to the NBOs as the NPA values were not reported.[4] The H still has a negative charge of −0.5*e* for either state, so the dominant electron configuration for the ground state of the cation is $Th^{2+}H^-$. The results for $ThH^{0/+/-}$ in terms of the charge distributions are consistent with these simple Th−H species not having any significant 5f character in the bonding, so Th should be considered to be transition metal-like rather than actinide-like.

The NBOs are consistent with the ThH^-/ThH photo-detachment spectrum, which has a large number of different states less than 2.65 eV. There are 18 states in ThH that can be formed on photo-detachment of an electron from ThH^- with detachment energies between 0.83 and 2.0 eV from the ground state of the anion. If we include electron detachment from the first excited state of the anion, there are a comparable number of predicted states as the first excited state of the anion is only 0.121 eV above the ground state at the CAS-PT2 level. As ThH bonding has a significant ionic component of the form Th^+H^-, there are 14 spin−orbit states in the Th^+ ion up to 1 eV derived from the $7s^26d^1$, $7s^25f^1$, $6d^3$, $7s^16d^15f^1$, and $7s^16d^2$ configurations. If ThH is considered to be totally covalent, then there are 11 Th neutral spin−orbit states in the first eV of excitation derived from the $7s^26d^2$, $7s^16d^3$, and $7s^16d^15f^1$ configurations of Th.

CONCLUSIONS

The nature of the bonding in compounds of the actinides is of broad interest. In the current work, the interaction of Th with H^-, H, and H^+ has been probed using a combination of high-level electronic structure calculations and experiments with experiments on the anion from the current work and on the cation from previous work by Armentrout and co-workers.[4] Due to the presence of a number of low-lying electronic states even with such a simple ligand, spin−orbit corrections are necessary to correctly predict the ground states of these diatomic molecules. At the SO-CASPT2 level, the ground state of ThH is predicted to be the $^2\Delta_{3/2}$ state ($7s^26d_\delta$ configuration) with the first $^2\Pi_{1/2}$ state ($7s^26d_\pi$ configuration) being only 0.043 eV higher in energy. CCSD(T) calculations without SO coupling predict these two states to be essentially degenerate, with the $^2\Pi$ state lower than the $^2\Delta$ state by 0.011 eV. At the FPD level with all of the electronic and ZPE contributions included, the $^2\Delta_{3/2}$ state is predicted to be the ground state for ThH with the $^2\Pi_{1/2}$ state being 0.069 eV higher in energy. The ground state for ThH^- is predicted to be $^3\Phi_2$ with a $7s^26d_\pi6d_\delta$ electron configuration. At the SO-CASPT2 level, the ground state of ThH^+ is predicted to be the $^3\Delta_1$ state ($7s6d_\delta$ electron configuration) with the first excited state, $^1\Sigma_0^+$, [$(7s + 6d)^2$ electron configuration] being only 0.025 eV higher in energy. In contrast, the CCSD(T) calculations without SO corrections predict the $^1\Sigma^+$ to be lower than the $^3\Delta$ state by 0.030 eV. At the FPD level with all of the electronic and ZPE contributions included, the $^3\Delta_1$ state is predicted to be the ground state for ThH^+ with the $^1\Sigma_0^+$ state being 0.096 eV higher in energy. Thus, inclusion of spin−orbit coupling is important as it can switch the ordering of the two lowest-energy states from what was obtained at the CCSD(T) level.

The adiabatic EA (AEA) is calculated as to be 0.820 eV at the FPD level, and the VDE is calculated to be 0.832 ± 0.02 eV. As the adiabatic EA and the VDE are comparable, we need to assign the peaks in the experimental photoelectron spectrum with reasonable intensity that are below the VDE down to almost 0.50 eV. Detachment of electrons from the ground state of the anion cannot account for the observed tail to lower EBE. Thus, transitions from Th^- might be present in this region of the spectrum, or there may be transitions from the two lowest-energy excited states of ThH^-, $^3\Sigma_0^-$ and $^3\Phi_3$, which are 0.121 and 0.244 eV, respectively, higher in energy than the ground state of ThH^-. It is also possible that vibrationally excited ThH^- could lead to lower detachment energies. The NBO results suggest that ThH has a significant contribution from the Th^+H^- ionic configuration. Thus, the ThH^- PES spectrum has many transitions that are consistent with excitations in Th^+ and/or Th. This suggests that use of H^- as a ligand bonded to an actinide atom in combination with PES and electronic structure calculations may serve as a probe of the excited states of the actinide positive ion and neutral.

The adiabatic IE of ThH at the FPD level is calculated to be 6.181 eV. As the IE of ThH and Th atom are calculated to be within 0.10 eV of each other, we suggest that the H^- does not change much as a ligand on ionization. The NBO results are consistent with a significant contribution of the Th^+H^- ionic configuration for the neutral, consistent with the PES results for the anion.

To provide additional insights into the bonding, the BDEs for ThH, ThH^-, and ThH^+ using the FPD approach were also calculated. The BDEs to the most stable species for ThH → Th + H, ThH^- → Th + H^-, and ThH^+ → Th^+ + H are all similar and fall in the energy range of 259−280 kJ/mol. The proton affinity of Th of 975.3 kJ/mol at 0 K is higher than that of NMe_3, showing that the atom is quite basic.[71] The current calculated BDE for ThH^+ differs from the previously determined experimental value for the BDE of ThH^+ by ~0.4 eV.[4] Prior CCSD(T) calculations[4] with an approximate SO contribution are consistent with the current calculations of the BDE of ThH^+. At this point, we do not understand the difference in the calculated and experimental values for the ThH^+ BDE, although we note that the differences in the experimental and computational FPD BDEs for other ThR^+ diatomics agree to better than 0.13 eV (12 kJ/mol).[8−11]

ASSOCIATED CONTENT

Supporting Information

The Supporting Information is available free of charge at https://pubs.acs.org/doi/10.1021/acs.jpca.1c07598.

Complete citations for refs 31 32, and 53, and total energy contributions using different basis sets (PDF)

https://doi.org/10.1021/acs.jpca.1c07598
J. Phys. Chem. A 2022, 126, 198−210

AUTHOR INFORMATION

Corresponding Authors

Kit H. Bowen − *Department of Chemistry, Johns Hopkins University, Baltimore, Maryland 21218, Unites States;* orcid.org/0000-0002-2858-6352; Email: kbowen@jhu.edu

David A. Dixon − *Department of Chemistry and Biochemistry, The University of Alabama, Tuscaloosa, Alabama 35401, Unites States;* orcid.org/0000-0002-9492-0056; Email: dadixon@ua.edu

Authors

Monica Vasiliu − *Department of Chemistry and Biochemistry, The University of Alabama, Tuscaloosa, Alabama 35401, Unites States*

Kirk A. Peterson − *Department of Chemistry, Washington State University, Pullman, Washington 99164, Unites States;* orcid.org/0000-0003-4901-3235

Mary Marshall − *Department of Chemistry, Johns Hopkins University, Baltimore, Maryland 21218, Unites States*

Zhaoguo Zhu − *Department of Chemistry, Johns Hopkins University, Baltimore, Maryland 21218, Unites States;* orcid.org/0000-0002-4395-9102

Burak A. Tufekci − *Department of Chemistry, Johns Hopkins University, Baltimore, Maryland 21218, Unites States*

Complete contact information is available at: https://pubs.acs.org/10.1021/acs.jpca.1c07598

Notes

The authors declare no competing financial interest.

ACKNOWLEDGMENTS

This work was supported by the U.S. Department of Energy (DOE), Office of Science, Office of Basic Energy Sciences, Heavy Element Chemistry program at Johns Hopkins University (K.H.B., experiment) through grant number, DE-SC0019317, the University of Alabama (D.A.D., computational) through grant through grant no. DE-SC0018921, and Washington State University (K.A.P., computational) through grant no. DE-SC0008501. D.A.D. thanks Robert Ramsay Fund at the University of Alabama.

REFERENCES

(1) Tang, R.; Si, R.; Fei, Z.; Fu, X.; Lu, Y.; Brage, T.; Liu, H.; Chen, C.; Ning, C. Candidate for Laser Cooling of a Negative Ion: High-Resolution Photoelectron Imaging of Th^-. *Phys. Rev. Lett.* **2019**, *123*, 203002.

(2) Zhu, Z.; Marshall, M.; Harris, R. M.; Bowen, K. H.; Vasiliu, M.; Dixon, D. A. Th_2O^-, Th_2Au^- and $Th_2AuO_{1,2}^-$ Anions: Photoelectron Spectroscopic and Computational Characterization of Energetics and Bonding. *J. Phys. Chem. A* **2021**, *125*, 258−271.

(3) Ciborowski, S. M.; Liu, G.; Blankenhorn, M.; Harris, R. M.; Marshall, M. A.; Zhu, Z.; Bowen, K. H.; Peterson, K. A. The Electron Affinity of the Uranium Atom. *J. Chem. Phys.* **2021**, *154*, 224307.

(4) Cox, R. M.; Armentrout, P. B.; de Jong, W. A. Reactions of Th^+ + H_2, D_2, and HD Studied by Guided Ion Beam Tandem Mass Spectroscopy and Quantum Chemical Calculations. *J. Phys. Chem. B* **2016**, *120*, 1601−1614.

(5) Cox, R. M.; Armentrout, P. B.; de Jong, W. A. Activation of CH_4 by Th^+ as Studied by Guided Ion Beam Mass Spectrometry and Quantum Chemistry. *Inorg. Chem.* **2015**, *54*, 3584−3599.

(6) Wang, X.; Andrews, L.; Gagliardi, L. Infrared Spectra of ThH_2, ThH_4, and the Hydride Bridging $ThH_4(H_2)_x$ (x = 1-4) Complexes in Solid Neon and Hydrogen. *J. Phys. Chem. A* **2008**, *112*, 1754−1761.

(7) Marshall, M.; Zhu, Z.; Harris, R.; Bowen, K. H.; Wang, W.; Wang, J.; Gong, C.; Zhang, X. ThH 5: An Actinide-Containing Superhalogen Molecule. *ChemPhysChem* **2021**, *22*, 5−8.

(8) Cox, R. M.; Citir, M.; Armentrout, P. B.; Battey, S. R.; Peterson, K. A. Bond Energies of ThO^+ and ThC^+: A Guided Ion Beam and Quantum Chemical Investigation of the Reactions of Thorium Cation with O_2 and CO. *J. Chem. Phys.* **2016**, *144*, 184309.

(9) Cox, R. M.; Kafle, A.; Armentrout, P. B.; Peterson, K. A. Bond Energy of ThN^+: A Guided Ion Beam and Quantum Chemical Investigation of the Reactions of Thorium Cation with N_2 and NO. *J. Chem. Phys.* **2019**, *151*, 034304.

(10) Kafle, A.; Armentrout, P. B.; Battey, S. R.; Peterson, K. A. Guided Ion Beam Studies of the Thorium Monocarbonyl Cation Bond Dissociation Energy and Theoretical Unveiling of Different Isomers of [Th,O,C]+ and Their Rearrangement Mechanism. *Inorg. Chem.* **2021**, *60*, 10426−10438.

(11) Armentrout, P. B.; Peterson, K. A. Guided Ion Beam and Quantum Chemical Investigation of the Thermochemistry of Thorium Dioxide Cations: Thermodynamic Evidence for Participation of f Orbitals in Bonding. *Inorg. Chem.* **2020**, *59*, 3118−3131.

(12) Thanthiriwatte, K. S.; Vasiliu, M.; Battey, S. R.; Lu, Q.; Peterson, K. A.; Andrews, L.; Dixon, D. A. Gas Phase Properties of MX_2 and MX_4 (X=F, Cl) for M = Group 4, Group 14, Ce, and Th. *J. Phys. Chem. A* **2015**, *119*, 5790−5803.

(13) Gerhards, M.; Thomas, O. C.; Nilles, J. M.; Zheng, W.-J.; Bowen, K. H. Cobalt-Benzene Cluster Anions: Mass Spectrometry and Negative Ion Photoelectron Spectroscopy. *J. Chem. Phys.* **2002**, *116*, 10247−10252.

(14) Ho, J.; Ervin, K. M.; Lineberger, W. C. Photoelectron spectroscopy of metal cluster anions: Cu_n^-, Ag_n^-, and Au_n^-. *J. Chem. Phys.* **1990**, *93*, 6987−7002.

(15) Purvis, G. D., III; Bartlett, R. J. A Full Coupled-Cluster Singles and Doubles Model: The Inclusion of Disconnected Triples. *J. Chem. Phys.* **1982**, *76*, 1910−1918.

(16) Raghavachari, K.; Trucks, G. W.; Pople, J. A.; Head-Gordon, M. A Fifth-order Perturbation Comparison of Electron Correlation Theories. *Chem. Phys. Lett.* **1989**, *157*, 479−483.

(17) Watts, J. D.; Gauss, J.; Bartlett, R. J. Coupled-Cluster Methods with Noniterative Triple Excitations for Restricted Open-Shell Hartree-Fock and Other General Single-Determinant Reference Functions. Energies and Analytical Gradients. *J. Chem. Phys.* **1993**, *98*, 8718−8733.

(18) Bartlett, R. J.; Musiał, M. Coupled-Cluster Theory in Quantum Chemistry. *Rev. Mod. Phys.* **2007**, *79*, 291−352.

(19) Douglas, M.; Kroll, N. M. Quantum Electrodynamical Corrections to the Fine Structure of Helium. *Ann. Phys.* **1974**, *82*, 89−155.

(20) Jansen, G.; Hess, B. A. Revision of the Douglas-Kroll Transformation. *Phys. Rev. A: At., Mol., Opt. Phys.* **1989**, *39*, 6016.

(21) Wolf, A.; Reiher, M.; Hess, B. A. The Generalized Douglas-Kroll Transformation. *J. Chem. Phys.* **2002**, *117*, 9215−9226.

(22) Kendall, R. A.; Dunning, T. H., Jr.; Harrison, R. J. Electron Affinities of the First-Row Atoms Revisited. Systematic Basis Sets and Wave Functions. *J. Chem. Phys.* **1992**, *96*, 6796−6806.

(23) De Jong, W. A.; Harrison, R. J.; Dixon, D. A. Parallel Douglas−Kroll Energy and Gradients in NWChem: Estimating Scalar Relativistic Effects Using Douglas−Kroll Contracted Basis Sets. *J. Chem. Phys.* **2001**, *114*, 48−53.

(24) Peterson, K. A. Correlation Consistent Basis Sets for Actinides. I. The Th and U Atoms. *J. Chem. Phys.* **2015**, *142*, 074105.

(25) Dunham, J. L. The Energy Levels of a Rotating Vibrator. *Phys. Rev.* **1932**, *41*, 721−731.

(26) Dunham, J. L. The Wentzel-Brillouin-Kramers Method of Solving the Wave Equation. *Phys. Rev.* **1932**, *41*, 713−720.

(27) Peterson, K. A.; Woon, D. E.; Dunning, T. H., Jr. Benchmark Calculations with Correlated Molecular Wave Function. IV. The Classical Barrier Height of the $H+H_2 \rightarrow H_2+H$ Reaction. *J. Chem. Phys.* **1994**, *100*, 7410−7415.

(28) Deegan, M. J. O.; Knowles, P. J. Perturbative Corrections to Account for Triple Excitations in Closed and Open Shell Coupled Cluster Theories. *Chem. Phys. Lett.* **1994**, *227*, 321−326.
(29) Rittby, M.; Bartlett, R. J. An Open-Shell Spin-Restricted Coupled Cluster Method: Application to Ionization Potentials in N_2. *J. Phys. Chem.* **1988**, *92*, 3033−3036.
(30) Knowles, P. J.; Hampel, C.; Werner, H.-J. Coupled Cluster Theory for High Spin, Open Shell Reference Wave Functions. *J. Chem. Phys.* **1993**, *99*, 5219−5227.
(31) Werner, H.-J.; Knowles, P. J.; Knizia, G.; Manby, F. R.; Schütz, M.; Celani, P.; Györffy, W.; Kats, D.; Korona, T.; Lindh, R.; et al. MOLPRO, version 2019.2, A Package of Ab Initio Programs. https://www.molpro.net (accessed 1 Jan, 2021).
(32) Werner, H.-J.; Knowles, P. J.; Manby, F. R.; Black, J. A.; Doll, K.; Heßelmann, A.; Kats, D.; Köhn, A.; Korona, T.; Kreplin, D. A.; et al. The Molpro Quantum Chemistry Package. *J. Chem. Phys.* **2020**, *152*, 144107.
(33) Roos, B. O.; Taylor, P. R.; Sigbahn, P. E. M. A Complete Active Space SCF Method (CASSCF) Using a Density-matrix Formulated Super-CI Approach. *Chem. Phys.* **1980**, *48*, 157−173.
(34) Siegbahn, P. E. M.; Almlöf, J.; Heiberg, A.; Roos, B. O. The Complete Active Space SCF (CASSCF) Method in a Newton-Raphson Formulation with Application to the HNO Molecule. *J. Chem. Phys.* **1981**, *74*, 2384−2396.
(35) Dunning, T. H., Jr. Gaussian basis set for use in correlated molecular calculations. I. The atoms boron through neon and hydrogen. *J. Chem. Phys.* **1989**, *90*, 1007−1023.
(36) Weigand, A.; Cao, X.; Hangele, T.; Dolg, M. Relativistic Small-Core Pseudopotentials for Actinium, Thorium, and Protactinium. *J. Phys. Chem. A* **2014**, *118*, 2519−2530.
(37) VanGundy, R. A.; Bartlett, J. H.; Heaven, M. C.; Battey, S. R.; Peterson, K. A. Spectroscopic and Theoretical Studies of ThCl and $ThCl^+$. *J. Chem. Phys.* **2017**, *146*, 054307.
(38) Barker, B. J.; Antonov, I. O.; Heaven, M. C.; Peterson, K. A. Spectroscopic Investigations of ThF and ThF^+. *J. Chem. Phys.* **2012**, *136*, 104305.
(39) Nguyen, D.-T.; Steimle, T.; Linton, C.; Cheng, L. Optical Stark and Zeeman Spectroscopy of Thorium Fluoride (ThF) and Thorium Chloride (ThCl). *J. Phys. Chem. A* **2019**, *123*, 1423−1433.
(40) Andersson, K.; Malmqvist, P. A.; Roos, B. O.; Sadlej, A. J.; Wolinski, K. Second-Order Perturbation Theory with a CASSCF Reference Function. *J. Phys. Chem.* **1990**, *94*, 5483−5488.
(41) Andersson, K.; Malmqvist, P. Å.; Roos, B. O. Second-Order Perturbation Theory with a Complete Active Space Self-Consistent Field Reference Function. *J. Chem. Phys.* **1992**, *96*, 1218−1226.
(42) Ghigo, G.; Roos, B. O.; Malmqvist, P.-Å. A Modified Definition of the Zeroth-Order Hamiltonian in Multiconfigurational Perturbation Theory (CASPT2). *Chem. Phys. Lett.* **2004**, *396*, 142−149.
(43) Berning, A.; Schweizer, M.; Werner, H.-J.; Knowles, P. J.; Palmieri, P. Spin-orbit matrix elements for internally contracted multireference configuration interaction wavefunctions. *Mol. Phys.* **2000**, *98*, 1823−1833.
(44) Dixon, D. A.; Feller, D.; Peterson, K. A. A Practical Guide to Reliable First Principles Computational Thermochemistry Predictions Across the Periodic Table. In *Annual Reports in Computational Chemistry*; Wheeler, R. A., Tschumper, G. S., Eds.; Elsevier: Amsterdam, 2012; Vol. *8*, Chapter 1, pp 1−28.
(45) Feller, D.; Peterson, K. A.; Dixon, D. A. Further Benchmarks of a Composite, Convergent, Statistically-Calibrated Coupled Cluster-Based Approach for Thermochemical and Spectroscopic Studies. *Mol. Phys.* **2012**, *110*, 2381−2399.
(46) Peterson, K. A.; Feller, D.; Dixon, D. A. Chemical Accuracy in Ab Initio Thermochemistry and Spectroscopy: Current Strategies and Future Challenges. *Theor. Chem. Acc.* **2012**, *131*, 1079.
(47) Feller, D.; Peterson, K. A.; Dixon, D. A. The Impact of Larger Basis Sets and Explicitly Correlated Coupled Cluster Theory on the Feller-Peterson-Dixon Composite Method. In *Annual Reports in Computational Chemistry*; Dixon, D. A., Ed.; Elsevier: Amsterdam, 2016; Vol. *12*, pp 47−78.
(48) Watts, J. D.; Bartlett, R. J. The Coupled-Cluster Single, Double, and Triple Excitation Model for Open-Shell Single Reference Functions. *J. Chem. Phys.* **1990**, *93*, 6104−6105.
(49) Noga, J.; Bartlett, R. J. The Full CCSDT Model for Molecular Electronic Structure. *J. Chem. Phys.* **1987**, *86*, 7041−7050.
(50) Kucharski, S. A.; Bartlett, R. J. Noniterative Energy Corrections through Fifth-Order to the Coupled Cluster Singles and Doubles Method. *J. Chem. Phys.* **1998**, *108*, 5243−5254.
(51) MRCC, A quantum chemical program suite (see also Rolik, Z.; Szegedy, L.; Ladjánszki, I.; Ladóczki, B.; Kállay, M. An Efficient Linear-Scaling CCSD(T) Method Based on Local Natural Orbitals. *J. Chem. Phys.* **2013**, *139*, 094105 as well as: www.mrcc.hu).
(52) Dyall, K. G. An Exact Separation of the Spin-Free and Spin-Dependent Terms of the Dirac-Coulomb-Breit Hamiltonian. *J. Chem. Phys.* **1994**, *100*, 2118−2127.
(53) Gomes, A. S. P.; Saue, T.; Visscher, L.; Jensen, H. J. A.; Bast, R. *DIRAC, a Relativistic Ab Initio Electronic Structure Program, Release DIRAC19*, 2019. available at http://dx.doi.org/10.5281/zenodo.3572669. See also http://www.diracprogram.org (accessed 1 April, 2021).
(54) Visscher, L.; Lee, T. J.; Dyall, K. G. Formulation and Implementation of a Relativistic Unrestricted Coupled-Cluster Method Including Noniterative Connected Triples. *J. Chem. Phys.* **1996**, *105*, 8769−8776.
(55) Visscher, L.; Eliav, E.; Kaldor, U. Formulation and Implementation of the Relativistic Fock-Space Coupled Cluster Method for Molecules. *J. Chem. Phys.* **2001**, *115*, 9720−9726.
(56) Fleig, T.; Olsen, J.; Marian, C. M. The Generalized Active Space Concept for the Relativistic Treatment of Electron Correlation. I. Kramers-Restricted Two-Component Configuration Interaction. *J. Chem. Phys.* **2001**, *114*, 4775−4790.
(57) Olsen, J.; Jørgensen, P.; Simons, J. Passing the One-Billion Limit in Full Configuration-Interaction (FCI) Calculations. *Chem. Phys. Lett.* **1990**, *169*, 463−472.
(58) Fleig, T.; Visscher, L. Large-Scale Electron Correlation Calculations in the Framework of the Spin-Free Dirac Formalism: The Au_2 Molecule Revisited. *Chem. Phys.* **2005**, *311*, 113−120.
(59) Pyykkö, P.; Zhao, L.-B. Search for Effective Local Model Potentials for Simulation of Quantum Electrodynamic Effects in Relativistic Calculations. *J. Phys. B: At., Mol. Opt. Phys.* **2003**, *36*, 1469−1478.
(60) Reed, A. E.; Curtiss, L. A.; Weinhold, F. Intermolecular Interactions from a Natural Bond Orbital, Donor-Acceptor Viewpoint. *Chem. Rev.* **1988**, *88*, 899−926.
(61) Weinhold, F.; Landis, C. R. *Valency and Bonding: A Natural Bond Orbital Donor-Acceptor Perspective*; University Press: Cambridge, U.K., 2005.
(62) Glendening, E. D.; Badenhoop, J. K.; Reed, A. E.; Carpenter, J. E.; Bohmann, J. A.; Morales, C. M.; Karafiloglou, P.; Landis, C. R.; Weinhold, F. *Natural Bond Order 7.0*; Theoretical Chemistry Institute, University of Wisconsin: Madison, WI, 2018.
(63) Glendening, E. D.; Landis, C. R.; Weinhold, F. NBO 7.0: New Vistas in Localized and Delocalized Chemical Bonding Theory. *J. Comput. Chem.* **2019**, *40*, 2234−2241.
(64) Kramida, A.; Ralchenko, Y.; Reader, J.; NIST ASD Team. *NIST Atomic Spectra Database*; National Institute of Standards and Technology: Gaithersburg, MD, 2020. (ver. 5.8), [online]. Available: https://physics.nist.gov/asdhttps://doi.org/10.18434/T4W30F [7 July, 2020].
(65) https://atct.anl.gov/Thermochemical%20Data/version%201.122g/index.php accessed Jan 18, 2019.
(66) Cox, J. D.; Wagman, D. D.; Medvedev, V. A. *CODATA Key Values for Thermodynamics*; Hemisphere Publishing Corp.: New York, 1989.
(67) Ruscic, B.; Pinzon, R. E.; Morton, M. L.; von Laszevski, G.; Bittner, S. J.; Nijsure, S. G.; Amin, K. A.; Minkoff, M.; Wagner, A. F. Introduction to Active Thermochemical Tables: Several "Key" Enthalpies of Formation Revisited. *J. Phys. Chem. A* **2004**, *108*, 9979−9997.

(68) Changala, P. B.; Nguyen, T. L.; Baraban, J. H.; Ellison, G. B.; Stanton, J. F.; Bross, D. H.; Ruscic, B. Active Thermochemical Tables: The Adiabatic Ionization Energy of Hydrogen Peroxide. *J. Phys. Chem. A* **2017**, *121*, 8799−8806.
(69) Curtiss, L. A.; Raghavachari, K.; Redfern, P. C.; Pople, J. A. Assessment of Gaussian-2 and Density Functional Theories for the Computation of Enthalpies of Formation. *J. Chem. Phys.* **1997**, *106*, 1063−1079.
(70) Wagman, D. D.; Evans, W. H.; Parker, V. B.; Schumm, R. H.; Halow, I.; Bailey, S. M.; Churney, K. L.; Nuttall, R. L. Erratum: The NBS tables of chemical thermodynamic properties. Selected values for inorganic and C1 and C2 organic substances in SI units [J. Phys. Chem. Ref. Data 11, Suppl. 2 (1982)]. *J. Phys. Chem. Ref. Data* **1989**, *18*, 1807−1812.
(71) Hunter, E. P. L.; Lias, S. G. Evaluated Gas Phase Basicities and Proton Affinities of Molecules: An Update. *J. Phys. Chem. Ref. Data* **1998**, *27*, 413−656.

https://doi.org/10.1021/acs.jpca.1c07598
J. Phys. Chem. A 2022, 126, 198−210